2

# One-dimensional Models for Diffusion and Segregation of Boron and for Ion Implantation of Aluminum in 4H-Silicon Carbide

Kazuhiro Mochizuki
*Central Research Laboratory, Hitachi, Ltd.*
*Japan*

## 1. Introduction

Silicon carbide with a poly-type 4H structure (4H-SiC) is an attractive material for power devices. While bipolar devices mainly utilize 4H-SiC p-n junctions, unipolar devices use p-n junctions both within the active region (to control the electric field distribution) and at the edges of the devices (to reduce electric-field crowding) (Baliga, 2005). In a p-type region, very high doping is necessary since common acceptors have deep energy levels (B: 0.3 eV; Al: 0.2 eV) (Heera et al., 2001). Boron is known to exhibit complex diffusion behaviour (Linnarsson et al., 2003), while aluminum has extremely low diffusivity (Heera et al., 2001). Precise modeling of boron diffusion and aluminum-ion implantation is therefore crucial for developing high-performance 4H-SiC power devices.

For carbon-doped silicon, a boron diffusion model has been proposed (Cho et al., 2007). Unfortunately, the results cannot be directly applied to boron diffusion in SiC because of the existence of silicon and carbon sublattices. In addition, knowledge of boron segregation in 4H-SiC is lacking, preventing improvement of such novel devices as boron-doped polycrystalline silicon (poly-Si)/nitrogen-doped 4H-SiC heterojunction diodes (Hoshi et al., 2007). Dopant segregation in elementary-semiconductor/compound-semiconductor heterostructures—in which point defects in an elementary semiconductor undergo a configuration change when they enter a compound semiconductor—has yet to be studied. A framework for such analysis needs to be provided.

With regards to aluminum distribution, to precisely design p-n junctions in 4H-SiC power devices, as-implanted profiles have to be accurately determined. For that purpose, Monte Carlo simulation using binary collision approximation (BCA) was investigated (Chakarov and Temkin, 2006). However, according to a multiday BCA simulation using a large number of ion trajectories, values of the simulated aluminum concentration do not monotonically decrease when the aluminum concentration becomes comparable to an n-type drift-layer-doping level (in the order of $10^{15}$ $cm^{-3}$). A continuous-function approximation, just like the dual-Pearson approach established for ion implantation into silicon (Tasch et al., 1989), is thus needed.

The historic development and basic concepts of boron diffusion in SiC are reviewed as follows. It took 16 years for the vacancy model (Mokhov et al., 1984) to be refuted by the

interstitial model (Bracht et al., 2000). A "dual-sublattice" diffusion modeling, in which a different diffusivity is assigned for diffusion via each sublattice, was proposed next. At the same time, a "semi-atomistic" simulation, in which silicon interstitials ($I_{Si}$) and carbon interstitials ($I_C$) are approximated as the same interstitials (I) and silicon vacancies ($V_{Si}$) and carbon vacancies ($V_C$) are approximated as the same vacancies (V), was performed (Mochizuki et al., 2009). Although this approximation originally comes from the limitation of a commercial process simulator, it contributes to reducing the number of parameters needed in an atomistic simulation using a continuity equation of coupling reactions between $I_{Si}$, $I_C$, $V_{Si}$, $V_C$, and diffusing species.

After boron diffusion in 4H-SiC is discusssed, boron diffusion and segregation in a boron-doped poly-Si/nitrogen-doped 4H-SiC structure are investigated by combining the model described above and a reported model of poly-Si diffusion sources (Lau, 1990). The results of an experiment to analyze boron-concentration profiles near the heterointerface are presented. Care is taken in this experiment to avoid implantation damage by using in-situ doped poly-Si instead of boron-implanted poly-Si.

The latter half of this chapter is an analysis and modeling of aluminum-ion implantation into 4H-SiC. Owing to the extremely low diffusivity of aluminum, multiple-energy ion implantation is required to produce SiC layers with an almost constant aluminum concentration over a designed depth. First, the influence of the sequence of multiple-energy aluminum implantations into 6H-SiC (Ottaviani et al., 1999) is explained. Next, the dual-Pearson model, developed for ion implantation into silicon, is reviewed (Tasch et al., 1989). The experimental, as well as Monte-Carlo-simulated, as-implanted concentration profiles of aluminum are then presented. After that, aluminum implantation at a single energy is modelled by using the dual-Pearson approach.

To indicate the future direction of modeling and simulation studies on p-type dopants in 4H-SiC, state-of-the-art two-dimensional modeling of aluminum-ion implantation is discussed at the end of this chapter. The modeling and simulation described in this chapter will also provide a framework for analyzing n-type dopants (e.g., nitrogen and phosphorous) in SiC, group-IV impurities (e.g., carbon and silicon) in III-V compound semiconductors (e.g., GaAs and InP), and diffusion and segregation of any dopants in elementary-semiconductor/compound-semiconductor heterostructures (e.g., Ge/GaAs and C/BN).

## 2. Boron Diffusion and Segregation

### 2.1 Boron diffusion in 4H-SiC

(a) Historic background

The first analysis of boron diffusion in SiC was based on a boron-vacancy model of 6H-SiC (Mokhov et al, 1984). Detailed analysis of the boron-concentration profiles in nitrogen-doped 4H- and aluminum-doped 6H-SiC, however, indicated that $I_{Si}$, rather than $V_{Si}$, controls the diffusion of boron (Bracht et al., 2000). The $I_{Si}$-mediated boron diffusion was then reconsidered in light of evidence of participation of $I_C$ (Rüschenschmidt et al., 2004). According to experiments on self-diffusion in isotopically enriched 4H-SiC, the diffusivities of $I_{Si}$ and $I_C$ are of the same order of magnitude, and it was proposed that under specific experimental conditions, either defect is strongly related to the preferred lattice site by boron. Theoretical calculations on 3C-SiC (Rurali et al., 2002; Bockstedte et al., 2003; Gao et

al., 2004) also showed that $I_{Si}$ and $I_C$ are far more mobile than $V_{Si}$ and $V_C$. Under the assumption that $I_{Si}$ and $I_C$ have the same mobility in 4H-SiC, boron diffusion, via $I_{Si}$ and $I_C$, can be simulated from a certain initial distributuion of point defects.

Boron-related centers in SiC are known to have two key characteristics: a shallow acceptor with an ionization energy of about 0.30 eV and a deep level with an ionization energy of about 0.65 eV (Duijin-Arnold et al., 1998). While the nature of the shallow acceptor defect is accepted as an off-center substitutional boron atom at a silicon site ($B_{Si}$) (Duijin-Arnold et al., 1999), that of the deep boron-related level is not clear. The $B_{Si}$-$V_C$ pair (Duijin-Arnold et al., 1998) was refuted by *ab initio* calculations that suggest a $B_{Si}$-$Si_C$ complex as a candidate (Aradi et al., 2001). In addition, candidates such as a substitutional boron atom at a carbon site ($B_C$) and a $B_C$-$C_{Si}$ complex were also put forward (Bockstedte et al., 2001). The boron-related deep center prevails in boron-doped 4H-SiC homoepitaxially experimentally grown under a silicon-rich condition (Sridhara et al., 1998), while similar experiments under a carbon-rich condition favor the shallow boron acceptor (Rüschenschmidt et al., 2004). Since the site-competition effect suggests that boron atoms can occupy both silicon- and carbon-related sites, it is assumed that the deep boron-related level originates from $B_C$ (Rüschenschmidt et al., 2004).

According to the theoretical results on 3C-SiC (Rurali et al., 2002; Bockstedte et al., 2003), a mobile boron defect is a boron interstitial ($I_B$) rather than a boron-interstitial pair , which is considered to mediate boron diffusion in silicon (Sadigh et al., 1999; Windl et al., 1999). Although it is ideal to simulate diffusion of $I_B$ in order to calculate boron-concentration profiles, the most relevant configuration of $I_B$ in 4H-SiC is still not clear. To reproduce the experimentally obtained boron-diffusion profiles for designing 4H-SiC power devices, a boron-interstitial-pair diffusion model in a commercial process simulator, which is optimized mainly for the use with silicon, is applied. The reported boron-concentration profiles in 4H-SiC (Linnarsson et al., 2003; Linnarsson et al., 2004) are taken as an example because the annealing conditions for high-temperature (500°C)-implanted (200 keV/$4\times10^{14}$ $cm^{-2}$) boron ions were systematically varied.

(b) Dual-sublattice diffusion modeling

It is assumed that $I_{Si}$ and $I_C$ diffuse on their own sublattices in accord with the theoretical calculation on 3C-SiC (Bockstedte et al., 2004). The kick-out reactions forming an $I_B$ from a boron atom at the silicon site ($B_{Si}$) and at the carbon site ($B_C$) are then expressed as

$$B_{Si} + I_{Si} \leftrightarrows I_B(\text{type-I}) \tag{1}$$

and

$$B_C + I_C \leftrightarrows I_B(\text{type-II}), \tag{2}$$

where the expression for the charge state is omitted. In the case of 3C-SiC, $I_B$(type-I) and $I_B$(type-II) can be a carbon-coordinated tetrahedral site, a hexagonal site, or a split-interstitial at the silicon site or the carbon site (Bockstedte et al., 2003). The reactions given by Eqs. (1) and (2) correspond to the following reactions in the boron-interstitial pair diffusion model (Bracht, 2007):

$$B_{Si}^{j} + I_{Si}^{m} \leftrightarrows (B_{Si}\, I_{Si})^{u} + (j + m - u)\, h^{+}, \tag{1a}$$

$$B_C{}^k + I_C{}^n \leftrightarrows (B_C\, I_C)^v + (k + n - v)\, h^+, \tag{2a}$$

with charge states $j, k, m, n, u, v \in \{0, \pm1, \pm2, \ldots\}$ and the holes $h^+$. According to the previous calculation (Bockstedte et al., 2003), $I_{Si}$ in 3C-SiC can be charged from neutral to +4, and $I_C$ from –2 to +2. If it is assumed that the variations in the charge states of $I_{Si}$ and $I_C$ in 4H-SiC are the same as those in 3C-SiC, the ranges of $m$ and $n$ in Eqs. (1a) and (2a) are limited to $m \in \{0, 1, 2, 3, \text{and } 4\}$ and $n \in \{0, \pm1, \text{and } \pm2\}$.

Boron diffusion in an epitaxially grown 4H-SiC structure with a buried boron-doped layer (Janson et al., 2003a) is modeled as shown in Fig. 1. In this case, the concentrations of point defects are considered to be in thermodynamic equilibrium. The Fermi model, in which all effects of point defects on dopant diffusion are built into pair diffusivities (Plummer et al., 2000), is thus applied. In the present case, the pair diffusivities are $(B_{Si}I_{Si})^u$ and $(B_CI_C)^v$ in eqs. (1a) and (2a). In general, when doping concentration exceeds intrinsic carrier concentration $n_i$ (Baliga, 2005), where

$$n_i\,(T) = 1.70\times10^{16}\, T^{1.5} \exp[(-2.08\times10^4) / T]\ (\text{cm}^{-3}), \tag{3}$$

diffusion becomes concentration-dependent (Plummer et al., 2000). Diffusivity $D$ of a pair (impurity A/interstitial I) is thus expressed as

$$D_{AI} = D_{AI}{}^0 + D_{AI}{}^+(p/n_i)^{+1} + D_{AI}{}^{++}(p/n_i)^{+2} + D_{AI}{}^-(p/n_i)^{-1} + D_{AI}{}^=(p/n_i)^{-2}, \tag{4}$$

where $p$ is hole concentration, and superscripts "++" and "=" traditionally stand for +2 and

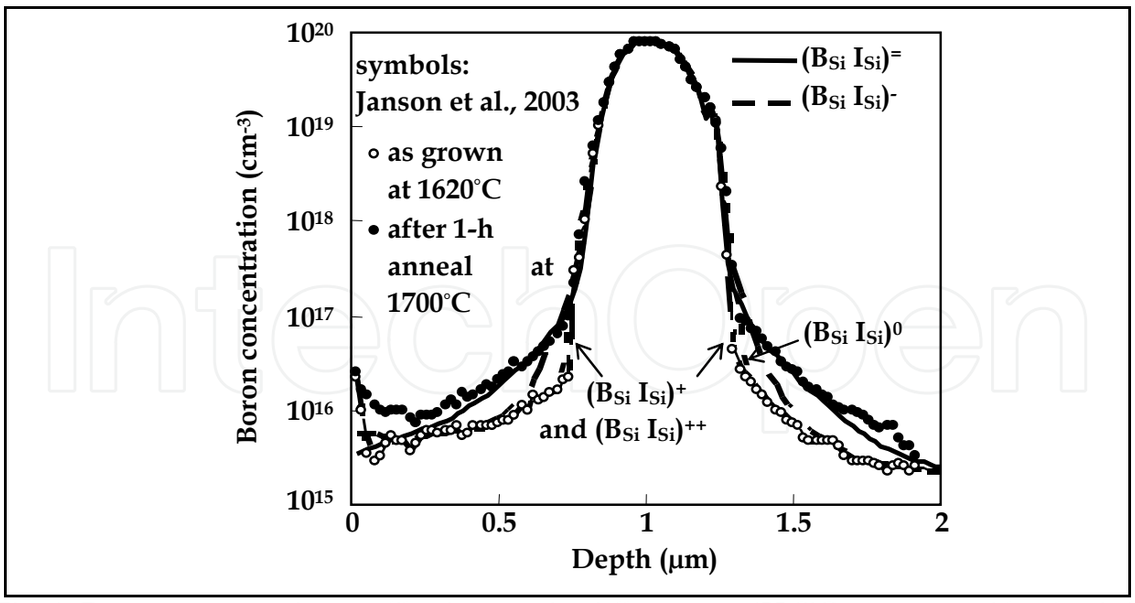


Fig. 1. Boron-concentration profiles in an epitaxially grown 4H-SiC structure with a buried boron-doped layer before (open circles) and after one-hour annealing at 1700°C [The profile simulated using diffusivity of a double-negatively charged $B_{Si}I_{Si}$ pair of $1\times10^{-15}$ cm$^2$/s (solid curve) can precisely reproduce the experimental results (solid circles).]

–2. As described in section **2.1**(a), boron atoms are incorporated into silicon sites as shallow acceptors ($B_{Si}^-$) when a SiC structure is grown under a carbon-rich condition. Equations (1a) and (4) thus become

$$B_{Si}^- + I_{Si}^m \leftrightarrows (B_{Si}\, I_{Si})^u + (-1 + m - u)\, h^+, \tag{5}$$

$$D_{(BSi\ ISi)} = D_{(BSi\ ISi)}^0 + D_{(BSi\ ISi)}^+ (p/n_i)^{+1} + D_{(BSi\ ISi)}^{++} (p/n_i)^{+2} + D_{(BSi\ ISi)}^- (p/n_i)^{-1} + D_{(BSi\ ISi)}^= (p/n_i)^{-2}, \tag{6}$$

with $m \in \{0, 1, 2, 3, \text{and } 4\}$ and $u \in \{0, \pm1, \text{and } \pm2\}$.
It is assumed that a single term in the right-hand side of Eq. (6) dominates the diffusion of ($B_{Si}I_{Si}$) pairs. The profile after one-hour annealing at 1700˚C in Fig. 1 was fitted by using one of the diffusivities of the following five ($B_{Si}I_{Si}$) pairs: of neutral, single- and double-positively charged, and single- and double-negatively charged. As shown in Fig. 1, the profile simulated with the diffusivity of a double-negatively-charged ($B_{Si}I_{Si}$) pair of $1\times10^{-15}$ cm²/s can precisely reproduce the experimentally obtained concentration profiles, while the profiles simulated using the other four diffusivities cannot. Therefore, $(B_{Si}I_{Si})^=$ is chosen to simulate the diffusion of $B_{Si}^-$.
The diffusion of $B_C$ (Bockstedte et al., 2003) is modeled next. Since $B_C$ can be regarded as an acceptor (Mochizuki et al., 2009), eq. (2a) becomes

$$B_C^- + I_C^n \leftrightarrows (B_C\, I_C)^v + (-1 + n - v)\, h^+, \tag{7}$$

with $n$ and $v \in \{0, \pm1, \text{and } \pm2\}$, and Eq. (4) becomes

$$D_{(BC\ IC)} = D_{(BC\ IC)}^0 + D_{(BC\ IC)}^+ (p/n_i)^{+1} + D_{(BC\ IC)}^{++} (p/n_i)^{+2} + D_{(BC\ IC)}^- (p/n_i)^{-1} + D_{(BC\ IC)}^= (p/n_i)^{-2}. \tag{8}$$

In p-type 6H-SiC, the diffusivity of in-diffused boron is proportional to $p$ when the boron vapor pressure is low (Mokhov et al., 1984). Under the assumption that similar dependence is observable in 4H-SiC, the diffusivity of a single-positively charged pair $(B_CI_C)^+$ is chosen to simulate the diffusion of $B_C^-$.

(c) Semi-atomistic diffusion simulation
Diffusion of implanted boron ions is calculated from the initial point-defect distribution determined by Monte-Carlo simulation. In the calculation, the continuity equation

$$\partial/\partial t\, (C_I + C_{(BSi\ I)}^= + C_{(BC\ I)}^+) = -\nabla \cdot (J_I + J_{(BSi\ I)}^= + J_{(BC\ I)}^+) - K_r\, (C_I\, C_V - C_I^*\, C_V^*) \tag{9}$$

is solved with

$$J_{(BSi\ I)}^= = -D_{(BSi\ I)}^= \{-\nabla [C_{BSi}^- (C_I / C_I^*) + C_{BSi}^- (C_I / C_I^*)\, (q\, E / k_B\, T)]\} \tag{10}$$

and

$$J_{(BC\ I)}^+ = -D_{(BC\ I)}^+ \{-\nabla [C_{BC}^- (C_I / C_I^*) + C_{BC}^- (C_I / C_I^*)\, (q\, E / k_B\, T)]\}, \tag{11}$$

where $C_I$ and $C_V$ are interstitial and vacancy concentrations, $C_I^*$ and $C_V^*$ are equilibrium interstitial and vacancy concentrations, $J_I$ is interstitial flux, $K_r$ is interstitial-vacancy bulk recombination coefficient, q is electronic charge, $E$ is electric field, $k_B$ is Boltzmann's

constant, and $T$ is absolute temperature. As expressed in eqs. (10) and (11), both the fluxes of $(B_{Si}I)^{=}$ and $(B_CI)^{+}$ take the effect of electric field into account.

The first step of the simulation is to obtain as-implanted boron profiles along with the initial distribution of point defects. As explained in section **2.1**(a), once $I_{Si}$ and $I_C$ are created, they are treated as the same I (with an unidentified origin). Similarly, the created $V_{Si}$ and $V_C$ are treated as the same V. Equations (6) and (8) are therefore simplified as

$$D_{(BSi\ I)} = D_{(BSi\ I)^{=}}(p/n_i)^{-2} \quad (12)$$

and

$$D_{(BC\ I)} = D_{(BC\ I)^{+}}(p/n_i)^{+1}. \quad (13)$$

In the Monte-Carlo simulation, the surface of 4H-SiC was assumed to be misoriented by 8° from (0001) toward [11-20], and the boron-ion-beam divergence was set to 0.1°.The probabilities of the implanted boron ions occupying a silicon site ($r_{Si}$) or a carbon site ($r_C$) are specified as follows. For 200 keV/$4\times10^{14}$ cm$^{-2}$ boron-ion implantation at 500°C (Linnarsson et al., 2003; Linnarsson et al., 2004), as-implanted concentration profiles of $B_{Si}^{-}$, $B_C^{-}$, I, and V are calculated under the tentative assumption that $r_{Si} = r_C = 0.5$ (Fig. 2).

The next step of the simulation is to solve Eq. (9). Both the time needed for increasing temperature before annealing and the time needed for decreasing temperature after annealing are neglected. Surface recombination of I and V, as well as surface evaporation of any species, are also neglected. The temperature dependences of $n_i$ in Eq. (3) and the diffusivity of I ($D_I$) (Rüschenschmidt et al., 2004), where

$$D_I(T) = 4.8 \exp[-7.6\ (\text{eV}) / k_B T]\ (\text{cm}^2/\text{s}), \quad (14)$$

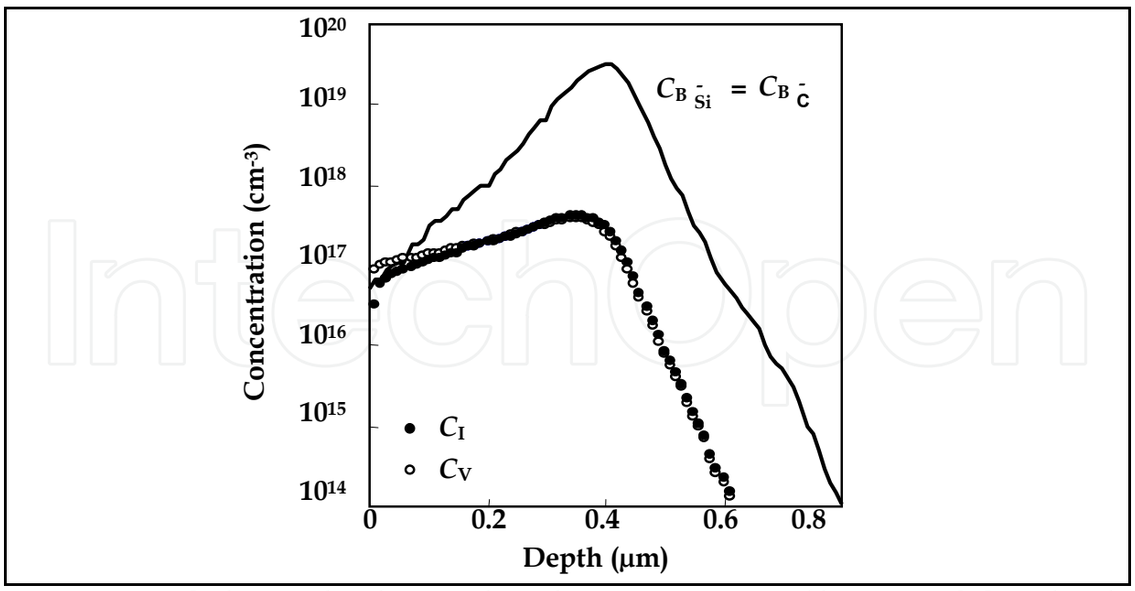


Fig. 2. Monte-Carlo simulated as-implanted concentration profiles in 4H-SiC under the assumption that the probability of implanted boron ions occupying a silicon site ($r_{Si}$) is 0.5 and that of occupying a carbon site ($r_C$) is 0.5

were used in the simulation. The diffusivity of V ($D_V$) was tentatively assumed to be the same as $D_I$, although the simulated profiles did not change with $D_V$.

Figure 3 shows simulated concentration profiles of $B_{Si}^-$, $B_C^-$, I, and V in the case of a background doping level $N_b$ of $2\times10^{15}$ cm$^{-3}$ (n-type), $T$ = 1900°C, and $t$ = 15 min (Linnarsson et al., 2004). According to the assumption made at the beginning of section **2.1**(b), the concentration profiles of $B_{Si}^-$ (dashed line) and $B_C^-$ (solid line) were obtained separately. Total boron concentration was thus calculated as the sum of the $B_{Si}^-$ and $B_C^-$ concentrations.

In Fig. 3, $C_I$ and $C_V$ become equilibrium values ($C_I^*$ and $C_V^*$, respectively) below a depth of 1.7 μm and are determined from the free energies of formation, $F_I$ and $F_V$, as follows (Bockstedte et al., 2003; Bracht, 2007):

$$C_I^* = C_{sI} \exp(-F_I / k_B T), \quad (15)$$

$$C_V^* = C_{sV} \exp(-F_V / k_B T), \quad (16)$$

where $C_{sI}$ and $C_{sV}$ are the concentrations of the sites that are open to Is and Vs, respectively. In the case of silicon, $C_{sI} = 5.0\times10^{22}$ cm$^{-3}$, $F_I$ = 2.36 eV, $C_{sV} = 2.0\times10^{23}$ cm$^{-3}$, and $F_V$ = 2.0 eV have been conventionally used in a commercial process simulator. Even with these values, it is possible to fit the simulated profiles to the reported boron-concentration profiles in 4H-SiC, except for the reciprocal dependence of boron diffusion on $p$ (Fig. 4). To explain the results in Fig. 4, the following values are employed: $C_{sI} = 4\times10^{30}$ cm$^{-3}$, $F_I$ = 5.2 eV, $C_{sV} = 2\times10^{33}$ cm$^{-3}$, and $F_V$ = 7.0 eV. The values of $F_I$ and $F_V$, theoretically calculated in the case of 3C-SiC, are, respectively, in the ranges of 4 to 14 eV and 1 to 9 eV (Bockstedte et al., 2003). However, the values of $C_{sI}$ and $C_{sV}$ are 8 to 10 orders of magnitude larger than those in the case of silicon (as discussed later in this section).

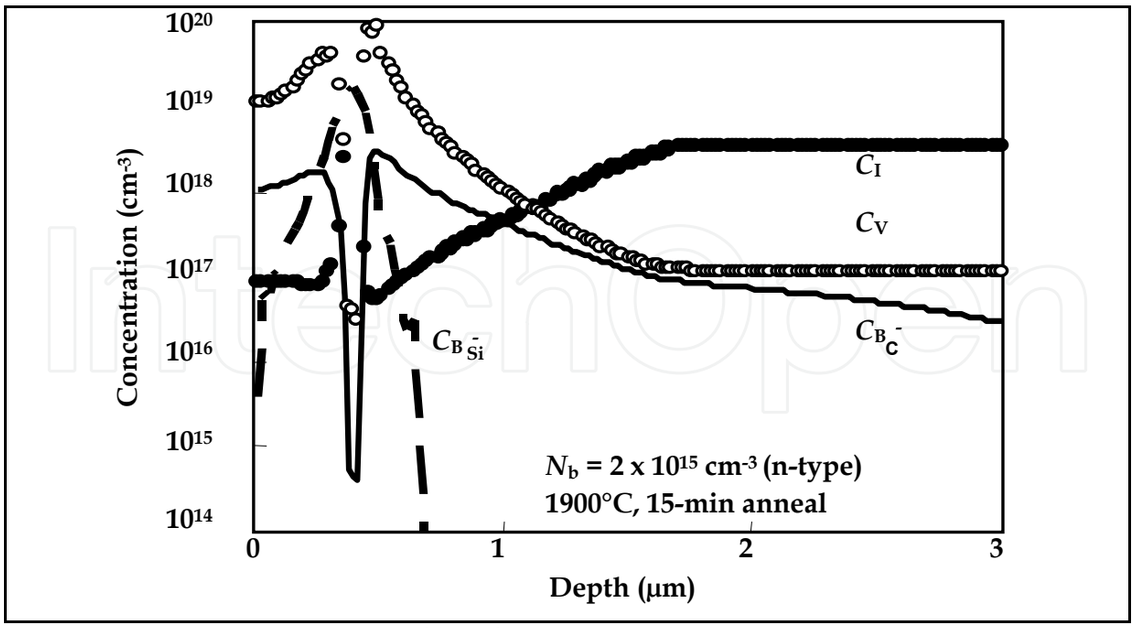


Fig. 3. Simulated concentration profiles of $B_{Si}^-$, $B_C^-$, I, and V in $2\times10^{15}$-cm$^{-3}$-doped n-type 4H-SiC after 15-min annealing at 1900°C simulated from the initial concentration profiles in Fig. 2

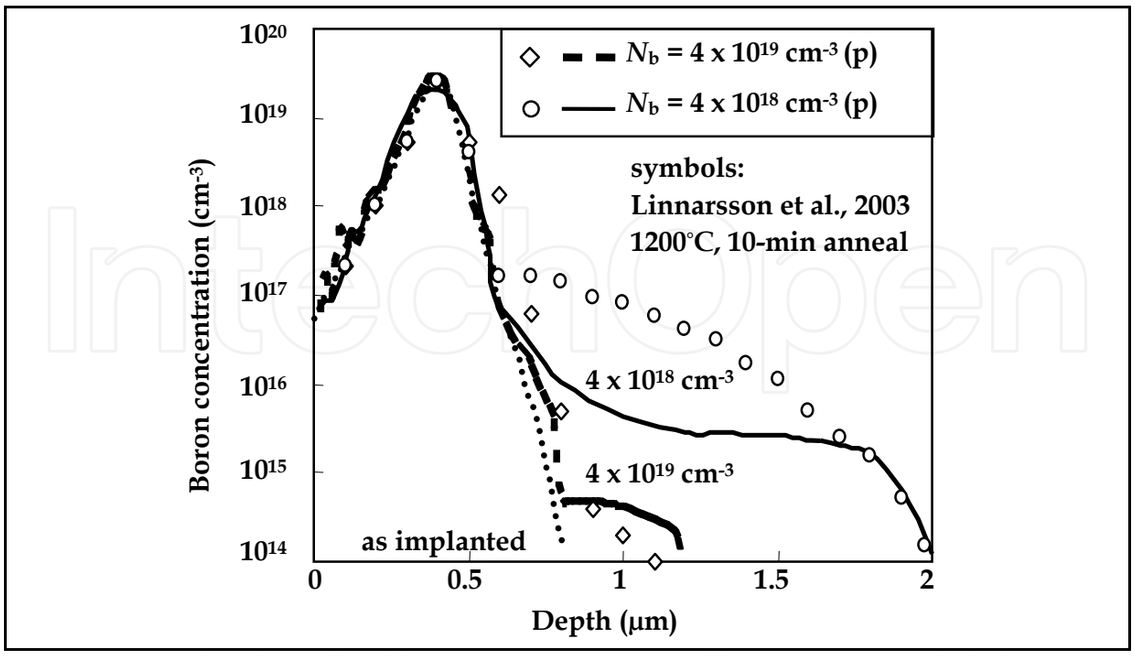


Fig. 4. Measured and simulated boron-concentration profiles in p-type 4H-SiC after 10-min annealing at 1200°C

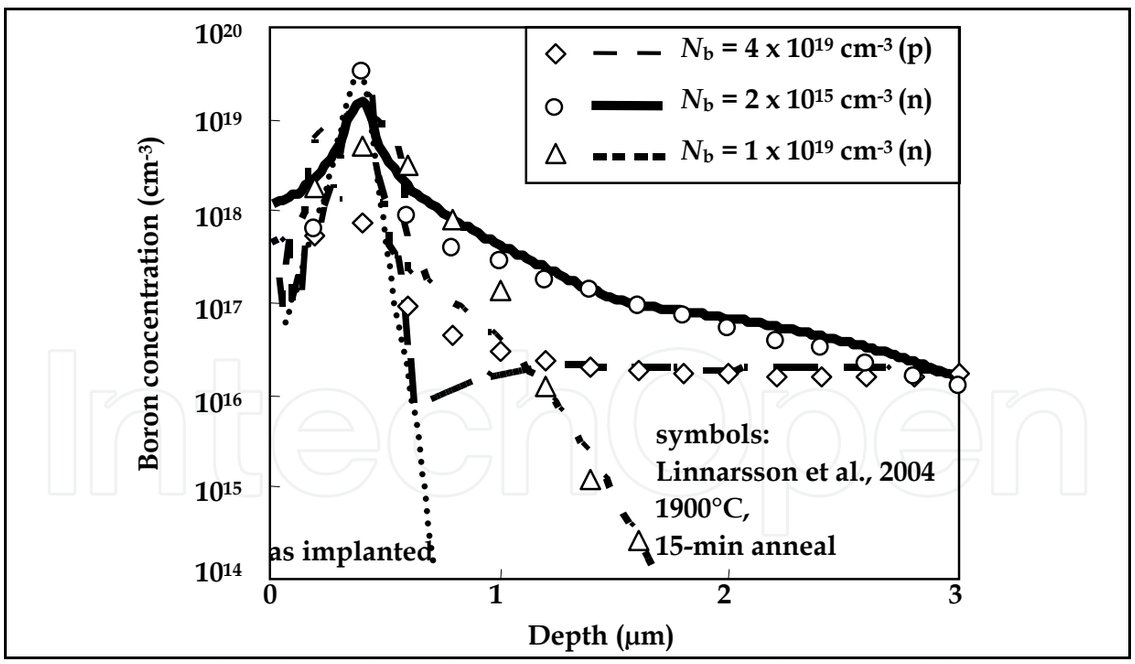


Fig. 5. Measured and simulated boron-concentration profiles in 4H-SiC after 15-min annealing at 1900°C

As shown in Fig. 5, owing to the introduction of the dual-sublattice modeling, the simulated boron-concentration profiles well describe the tail regions of the measured profiles (symbols) with background doping ranging from n- to p-type under conditions $T$ = 1900°C

and $t$ = 15 min (Linnarsson et al., 2004). The fitting parameters used are the same as those for Fig. 3. The tail regions are represented mainly by $B_{Si}^-$ [$N_b$ = 1×10$^{19}$ cm$^{-3}$ (n-type)] and $B_C^-$ [$N_b$ = 2×10$^{15}$ cm$^{-3}$ (n-type) and 4×10$^{19}$ cm$^{-3}$ (p-type)].

To use the modeling (section **2.1**(b)) and simulation described here for optimizing the boron-diffusion process in regards to device fabrication, time-dependent diffusion has to be accurately simulated. Figure 6 shows annealing-time (5 ot 90 min) dependences of boron-concentration profiles for $N_b$ = 4×10$^{19}$ cm$^{-3}$ (p-type) and $T$ = 1400°C (Linnarsson et al., 2004). The measured time-dependent boron-diffusion profiles (symbols) are precisely reproduced with the parameters $D_{(BSi\ I)^=}$ = 3×10$^{-18}$ cm$^2$/s, $D_{(BC\ I)^+}$ = 6×10$^{-12}$ cm$^2$/s, and $K_r$ = 3×10$^{-16}$ cm$^3$/s and the parameters expressed by Eqs. (3) and (14).

One of the biggest challenges in understanding boron diffusion in 4H-SiC has been its reciprocal dependence on $p$, observed in the case of $N_b$ = 4×10$^{18}$ and 4×10$^{19}$ cm$^{-3}$ (p-type), $T$ = 1200°C, and $t$ = 10 min (symbols in Fig. 4). Even when the diffusivity of $(B_CI)^+$, which is proportional to $p$ under thermodynamical equilibrium [Eq. (13)], is used, the dependence (Linnarsson et al., 2003) was successfully demonstrated, at least in the tail regions, with the parameters $D_{(BSi\ I)^=}$ = 4×10$^{-20}$ cm$^2$/s, $D_{(BC\ I)^+}$ = 4×10$^{-12}$ cm$^2$/s, and $K_r$ = 6×10$^{-16}$ cm$^3$/s and the parameters expressed in Eqs. (3) and (14). According to the theoretical calculation (Bockstedte et al., 2003), a variety of $I_{Si}$, $I_C$, $V_{Si}$, and $V_C$ exists in 3C-SiC. If it is assumed that a similar variety of point defects also exists in 4H-SiC, it is possible that the values of $C_I^*$ and $C_V^*$ in 4H-SiC are much larger than those in silicon at the same temperature. Since Fig. 5 is the only experimental result showing the reciprocal dependence of diffusivity of boron on $p$, further experimental investigation is needed to revise the parameters $C_{sI}$ and $C_{sV}$.

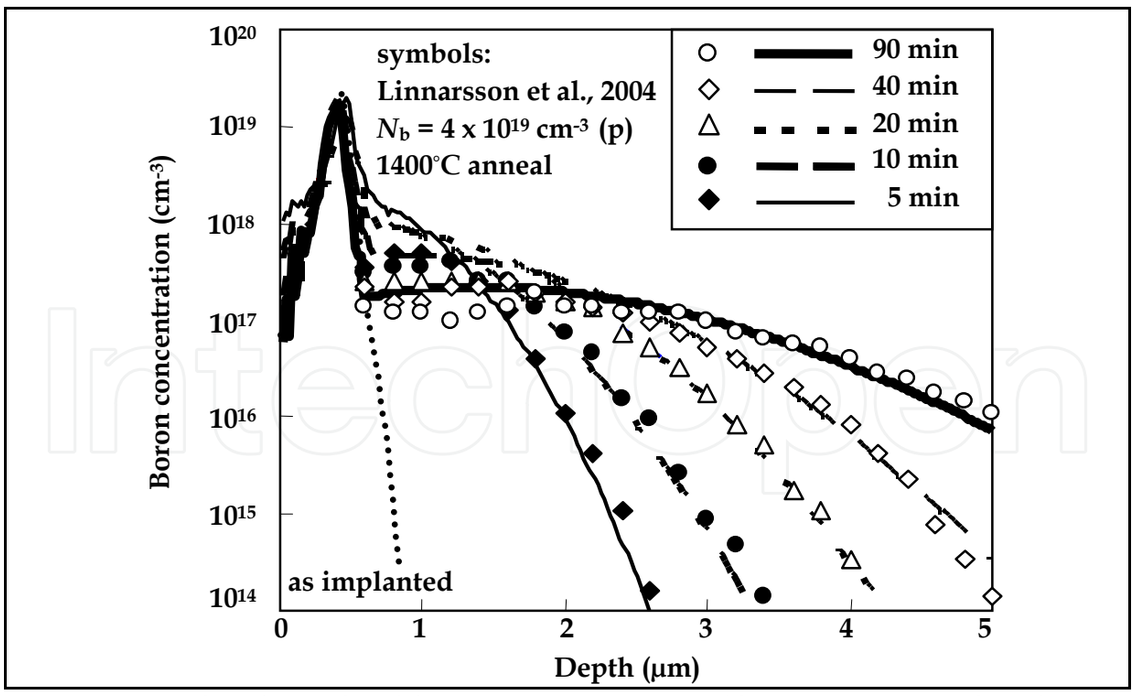


Fig. 6. Measured and simulated boron-concentration profiles in 4×10$^{19}$-cm$^{-3}$-doped p-type 4H-SiC after annealing at 1400°C

The following remaining issue should also be noted: optimization of $r_{Si}/r_C$ for applying the developed semi-atomistic simulation to fit other experimentally obtained boron-concentration profiles. Since this optimization is strongly related to experimental conditions (Rüschenschmidt et al., 2004), $r_{Si}/r_C$ needs to be optimized for each experimental condition.

### 2.2 Boron Diffusion and Segregation in Poly-Si/4H-SiC Structures

Diffusivities of a double-negatively charged B-$I_{Si}$ pair and a single-positively charged B-$I_C$ pair are extrapolated to less than 1000°C. Since the former diffusivity results in quite small values (Fig. 7), only the latter diffusivity is taken into account. Furthermore, only $I_C$s coming from carbon atoms in native oxides that remained on 4H-SiC are treated since the diffusivity of $I_C$ is also negligible (Rüschenschmidt et al., 2004).

(a) Model description

In regard to poly-silicon, three contributions to total boron concentration ($C_B$) were considered (Lau, 1990): active ($C_{ga}$) and inactive ($C_{gi}$) boron concentrations in grains, and boron concentration in grain boundaries ($C_b$). Since $C_B$ was chosen to be $3\times10^{20}$ cm$^{-3}$, which is larger than the maximum active concentration ($C_{Si}^{sat}$), $C_{ga} = C_{Si}^{sat}$; in the case of a poly-Si/Si structure, $k = C_{Si}^{sat}/C_{gi}$ [Fig. 8(a)].

In the case of a poly-Si/4H-SiC structure, $C_{gi}$ profiles in poly-Si were calculated by using boron-interstitial pair diffusivities one hundred times larger than those in single-crystalline silicon (Plummer et al., 2000). In the case of 4H-SiC, $C_{SiC}^{sat}$ is extrapolated, for example, to $4\times10^{16}$ cm$^{-3}$ at 850°C (Linnarsson et al., 2006). In accordance with the condition of $k$, as well as on the extent of diffusion of active ($C_a$) and inactive boron concentrations ($C_i$), $C_B$ profiles change, as illustrated in Fig. 8(a) for silicon and in Figs. 8(b) to (d) for 4H-SiC.

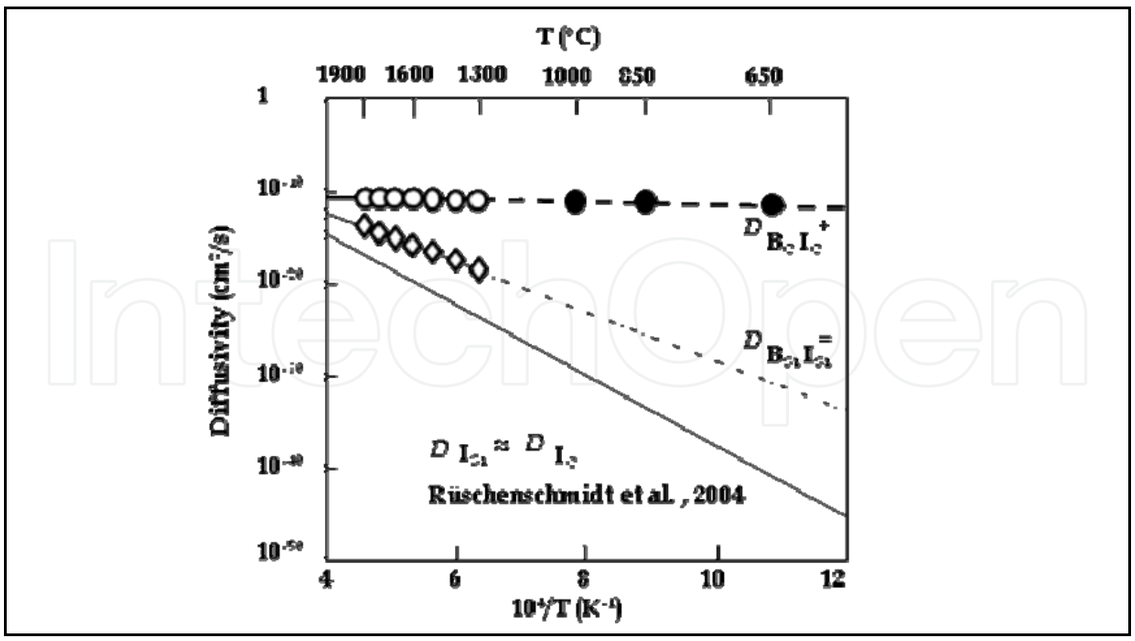


Fig. 7. Diffusivities of silicon and carbon interstitials ($I_{Si}$ and $I_C$), double-negatively charged boron-$I_{Si}$ pair, and single-positively charged boron-$I_C$ pair (Open and closed symbols denote values used in section **2.1** and in this section, respectively.)

(b) Experiments and discussion

A 200-nm-thick boron-doped amorphous silicon film was formed on nitrogen-doped 4H-SiC (0001) substrates by chemical vapour deposition at 350°C. Annealing for post-crystallization in nitrogen ambient was performed, followed by in-depth concentration-profile analysis using an 8-keV $O_2^+$ beam in a secondary-ion mass spectrometer (SIMS).

Measured $C_B$ profiles show a peak at the heterointerfaces but no tails corresponding to $C_{SiC}^{sat}$ (Fig. 9). This result indicates that inactive boron atoms with $k > 1$ (Fig. 8(c)) dominate boron diffusion and segregation. Under the assumption that the charge states of inactive boron atoms are neutral, $C_B$ profiles of poly-Si/4H-SiC pn diodes annealed at 850°C for 30

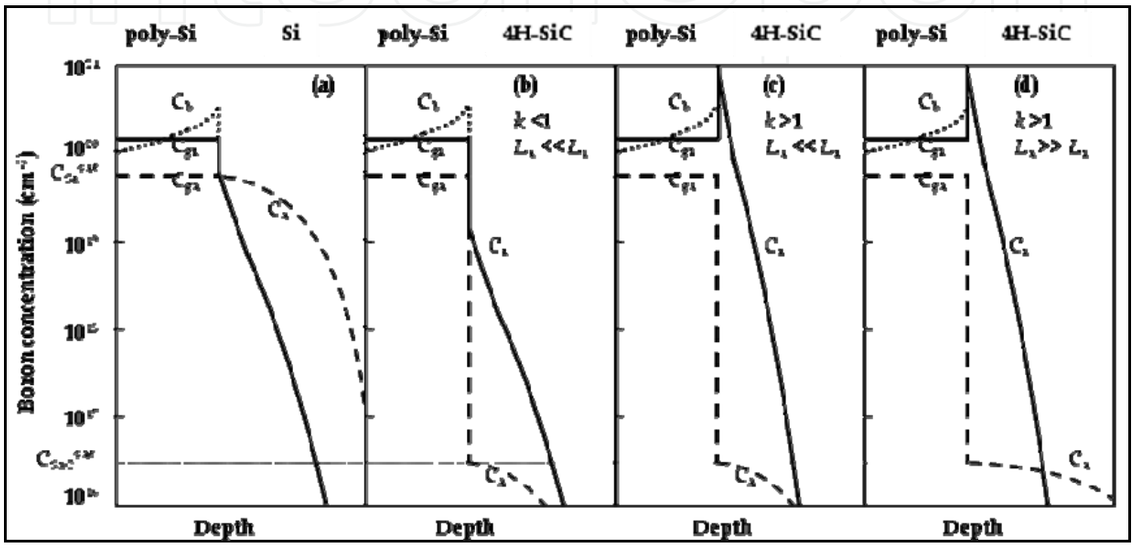


Fig. 8. Schematic illustrations of boron-concentration profiles in (a) poly-Si/Si and (b)–(d) poly-Si/4H-SiC pn diodes. In poly-Si/4H-SiC diodes, (b) corresponds to the case where segregation coefficient $k$ is less than unity, and (c) and (d) correspond to the case that $k > 1$. When the diffusion length of active boron atoms ($L_a$) is much less than the diffusion length of inactive boron atoms ($L_i$), profiles of inactive boron concentration ($C_i$) dominate profiles of total boron concentration ($C_B$) in 4H-SiC ((b) and (c)); on the other hand, when $L_a$ is much larger than $L_i$, profiles of active boron concentration ($C_a$) dominate the tail region of $C_B$ profiles for 4H-SiC, as shown in (d).

$C_{ga}$: active boron concentration in grains; $C_{gi}$: inactive boron concentration in grains;
$C_b$: boron concentration at grain boundaries; $C_{Si}^{sat}$: maximum active boron concentration in silicon; $C_{SiC}^{sat}$: maximum active boron concentration in 4H-SiC.

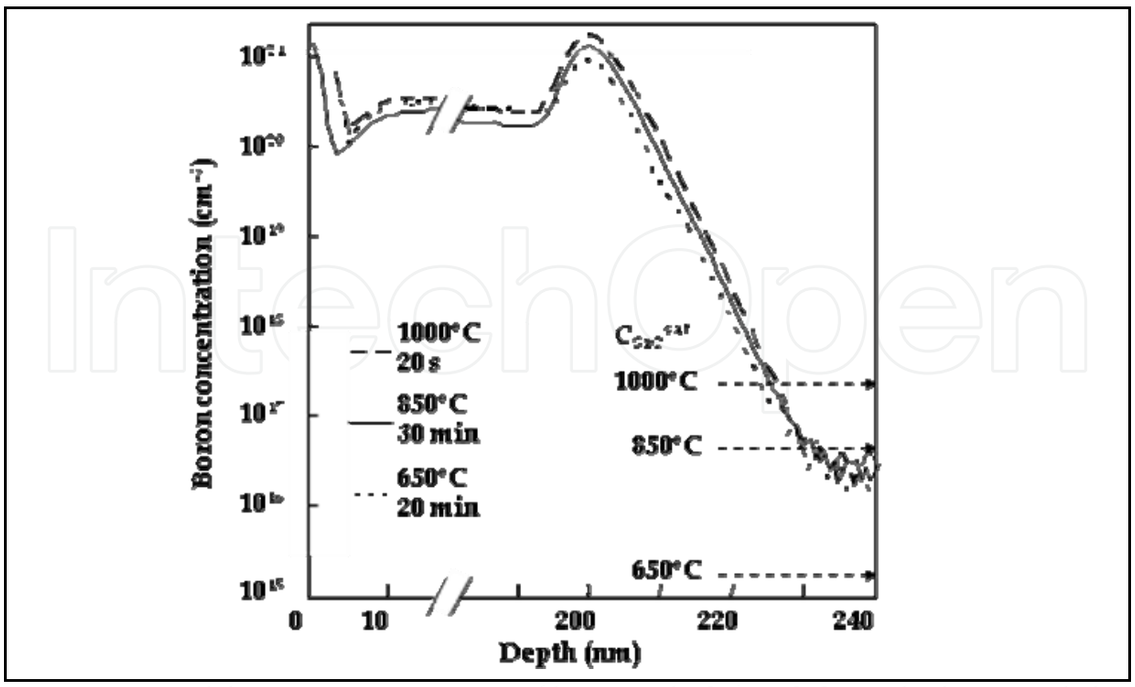


Fig. 9. Measured boron-concentration profiles in poly-Si/4H-SiC pn diodes annealed at 650–1000°C in nitrogen ambient

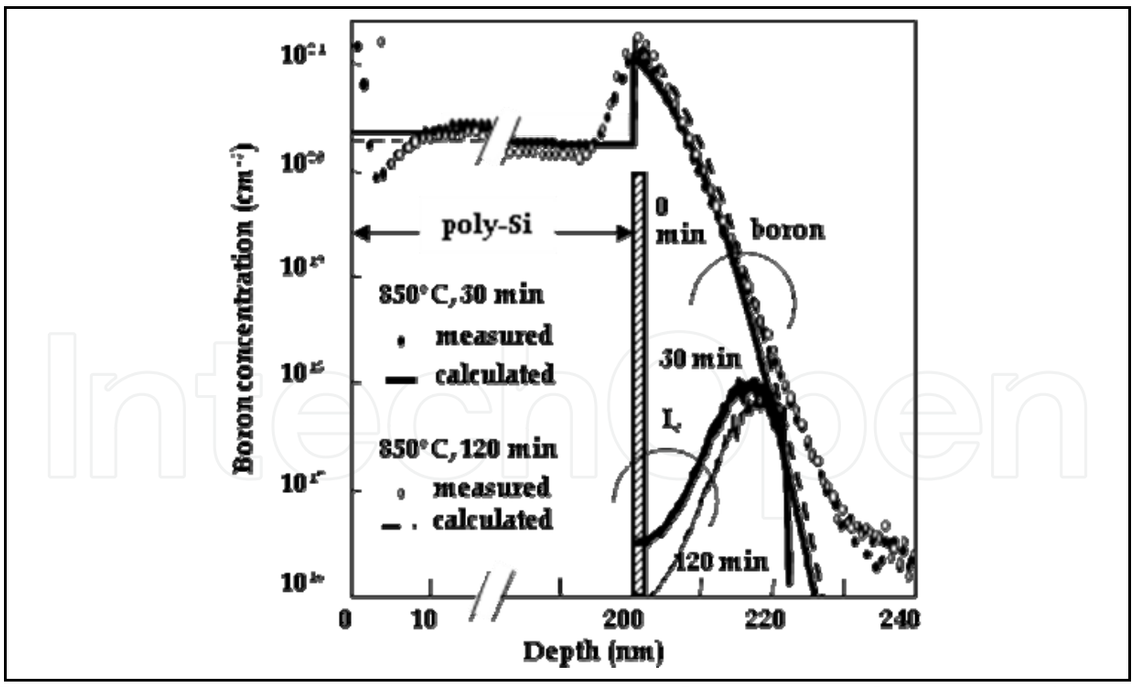


Fig. 10. Concentration profiles of boron and caluculated $I_C$ assuming an Interstitial $1\times10^{13}$ $cm^{-2}$ $I_C$ at the heterointerface [Interstitial-vacancy bulk recombination coefficient and equilibirium $I_C$ concentration are extrapolated from the reported results (Mochizuki et al., 2009).]

and 120 min were calculated. Initial sheet concentration of $I_C$ ($N_s$) of $1\times10^{13}$ $cm^{-2}$ at the heterointerface was found to reproduce the measured profiles, which show slight dependence on annealing time (Fig. 10). This $N_s$ value was thus used to determine $k$ in the temperature range of 650−1000°C (Mochizuki et al, 2010).

At 850°C, $k$ of 6.7 is much larger than 0.7 for poly-Si/Si at 900°C (Rausch et al., 1983) and 1.7 for Si/3C-$Si_{0.996}C_{0.004}$ at 850°C (Stewart et al., 2005) (Fig. 11). The increased driving force for boron segregation with carbon mole fraction seems to support the previous model, in which boron is trapped at a carbon-related defect (Stewart et al., 2005). However, the positive activation energy of $k$ (Fig. 12) indicates that a direct boron-carbon interaction (Liu et al., 2002) contributes to boron segregation. A recent report on suppression of boron diffusion by additional implantation of carbon (Tsirimpis et al, 2010) also supports the mechanism of direct boron-carbon interaction.

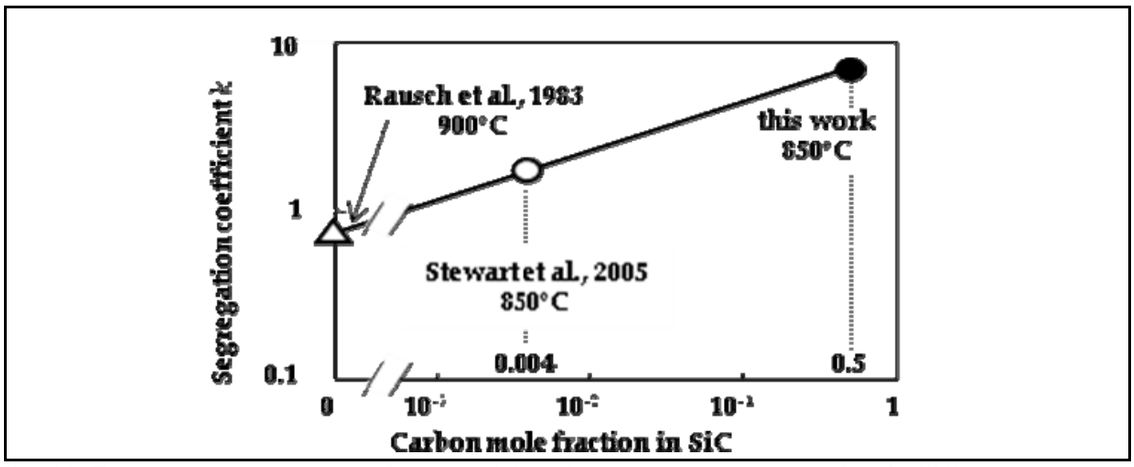


Fig. 11. Dependence of segregation coefficient $k$ on carbon mole fraction in SiC

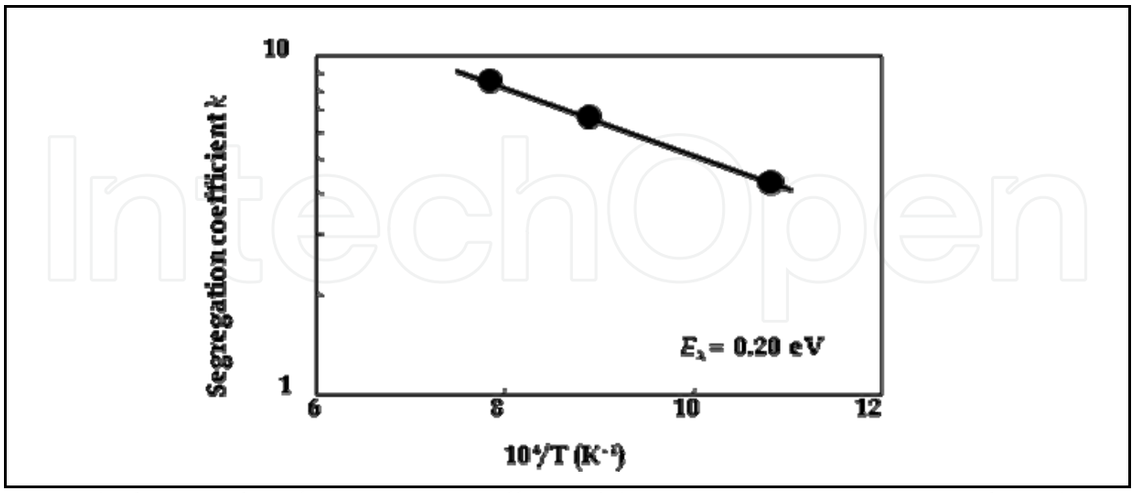


Fig. 12. Arrhenius plot of segregation coefficient $k$ (positive activation energy is shown)

## 3. Aluminum-ion Implantation

(a) Historic background

The effect of a sequence of multiple-energy aluminum implantations into 6H-SiC on channeling was reported (Ottaviani et al., 1999). In that report, "scatter-in" channeling did not occur because of less channeling in the case of increasing order of implantation energy. Scatter-in channeling was first observed in boron implantation into silicon and was called "paradoxical profile broadening" (Park et al., 1991). That can occur during high-tilt-angle implantation (e.g., 7° for (100) Si) through a randomized surface layer. In the scatter-in process, some high-energy ions, which move in a random direction after crossing the surface layer, are scattered in a channeling direction and penetrate deeper into the undamaged underlying crystal. The reduced aluminum channeling in the case of increasing order of implantation energy was attributed to the amorphization caused by one implantation affecting the subsequent implantation (Ottaviani et al., 1999).

In the case of boron implantation into (100) Si, the influence of surface oxide layer is crucial (Morris et al., 1995). When the tilt angle is 0°, the depth of the as-implanted profile decreases with increasing oxide thickness because a well-collimated ion beam is scattered by the amorphous oxide layer. On the other hand, at higher tilt angles and at certain energies, the as-implanted profile becomes deeper with increasing oxide thickness because of the scatter-in channeling. In the case of aluminum implantation into 4H- and 6H-SiC, the substrate is usually misoriented from (0001) by 4°−8° to achieve step-flow epitaxial growth (Kuroda et al., 1987). Thus, there is such a high probability of the scatter-in channeling of aluminum that the effect of a surface oxide on channeling has to be calculated and demonstrated.

(b) Experiments

Experimental sample preparation was started by forming a 35-nm-thick $SiO_2$ layer by plasma-enhanced chemical-vapour deposition, on a 50.8-mm-thick 4H-SiC wafer misoriented by 8° from (0001) toward [11-20]. The $SiO_2$ layer was then removed from half of the wafer using a solution of buffered hydrofluoric acid. Subsequently, five-fold aluminum implantation was carried out at RT to achieve 0.3-μm-deep boxlike profiles with a mean plateau concentration of $1\times10^{19}$ $cm^{-3}$. Implantation energies (keV) and corresponding doses ($\times10^{13}$ $cm^{-2}$) were 220/10, 160/5, 110/7, 70/6, and 35/3. A mechanical mask was used to form the following four implanted areas on the same wafer: without the $SiO_2$ layer in the case of decreasing order of implantation energy, without the $SiO_2$ layer in the case of increasing order of implantation energy, with the $SiO_2$ layer in the case of decreasing order of implantation energy, and with the $SiO_2$ layer in the case of increasing order of implantation energy.

To determine in-depth concentration profiles, SIMS analyses were carried out using an 8-keV $O_2^+$ beam. In addition to the experimentally obtained data, Monte-Carlo simulation using BCA was also utilized (Mochizuki and Onose, 2007).

The range parameters for Pearson frequency-distribution functions (Pearson, 1895) are sensitive to differences in SIMS background concentration levels (Janson et al., 2003b). Accordingly, the SIMS measured background levels ($5\times10^{14}$−$1\times10^{15}$ $cm^{-3}$) were subtracted from the SIMS measured depth profiles of aluminum concentrations. The resultant depth profiles are compared to the BCA-simulated ones in Fig. 13. Very good agreements of the computationally obtained profiles with the experimentally determined ones confirm that the BCA simulation can be used to generate quasi-experimental data.

The BCA profiles in Figs. 13(a) to (d) are thus redrawn in Fig. 14. They demonstrate that the implantation without the $SiO_2$ layer in a decreasing energy order resulted in the least extended tail in the aluminum-concentration profiles. In the case of decreasing order of implantation energy, the tail is mainly determined by aluminum concentration profiles formed during the first energy step (220 keV). The tail of profiles for implantation with the $SiO_2$ layer extends deeper than that for implantation without the $SiO_2$ layer. This difference probably results from the scatter-in channeling. In the case of increasing order of implantation energy, on the other hand, little difference in the tail is observed between profiles for implantaions with and without the $SiO_2$ layer. Thus, the effect of the reported amorphization-suppressed channeling (Ottaviani et al., 1999) is considered to be less than that of the scatter-in channeling (as discussed later). The difference between the reported results (Ottaviani et al., 1999) and our results might be related to the differences in the tilt (3.5° vs. 8°) and rotation angles (–90° vs. 0°) during implantation (although that reasoning is yet to be confirmed).

(c) Dual-Pearson model

Pearson frequency distribution functions (Pearson, 1895) have been successfully applied to represent a wide selection of implanted ion profiles in 4H-SiC (Janson et al., 2003b). For such heavy ions as aluminum, however, large channeling tails of distributions deviate from the single-Pearson functions (Janson et al., 2003; Stief et al. 1998; Lee and Park, 2002). The

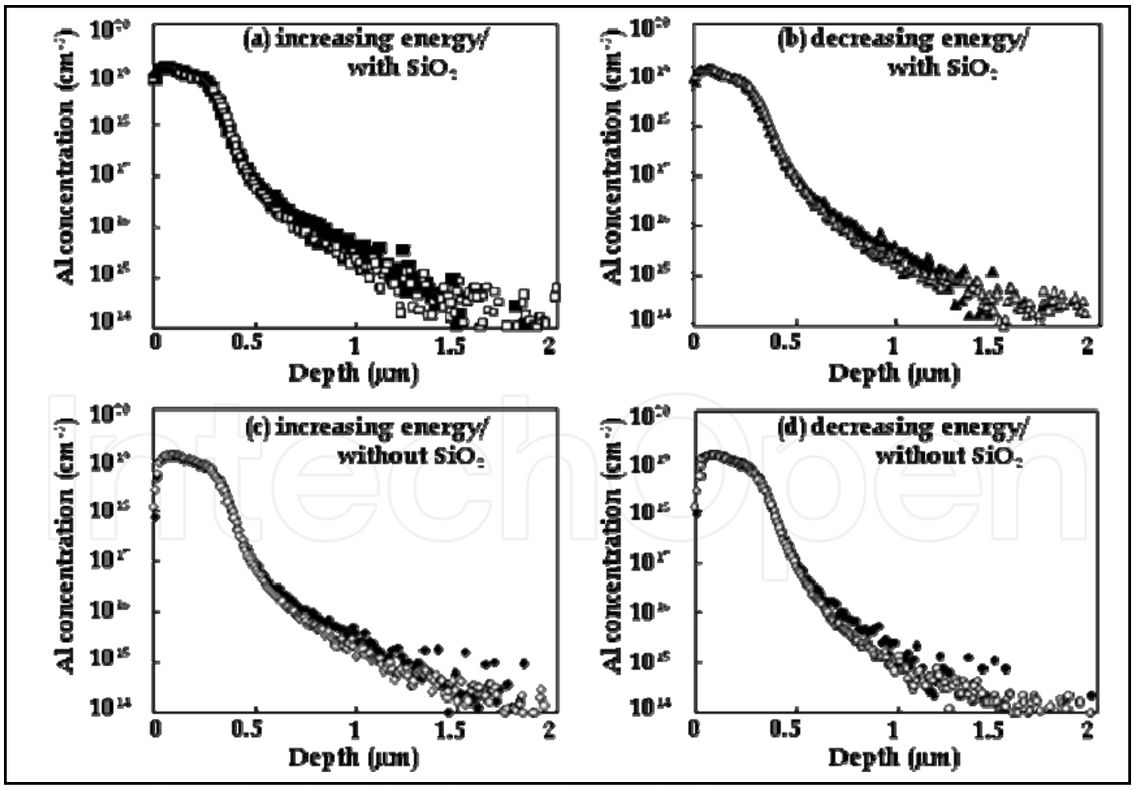


Fig. 13. Depth profiles of (solid symbols) background-subtracted SIMS-measured and (open symbols) BCA-simulated concentration profiles of five-fold aluminum implantation into 4H-SiC

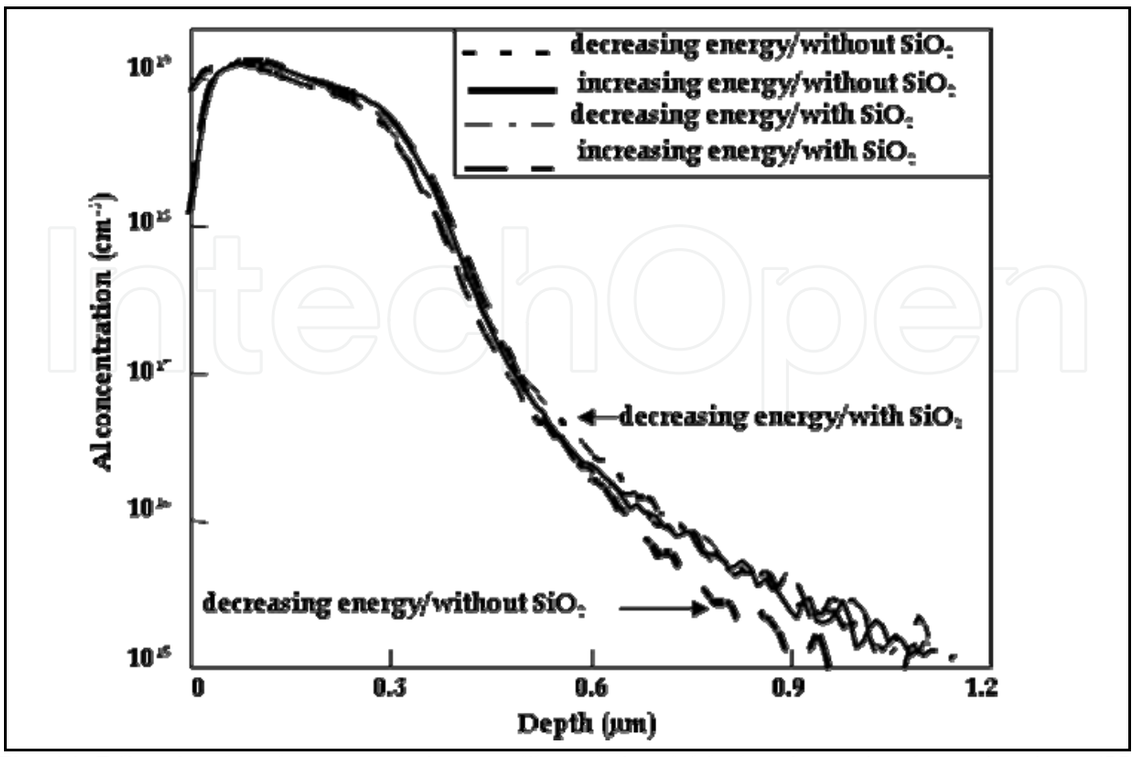


Fig. 14. BCA-simulated concentration profiles of five-fold aluminum implantation into 4H-SiC shown in Figs. 13(a) to (d)

dual-Pearson approach is thus extended to model the BCA-simulated profiles of aluminum implantations into 4H-SiC through a 35-nm-thick $SiO_2$ layer (Mochizuki and Onose, 2007) to implantations without the $SiO_2$ layer.

The dual-Pearson distribution is a weighted sum of two Pearson IV functions (Pearson, 1895) used to model the randomly scattered portion and the channeled portion of the profile (Morris et al., 1995). The depth profile of aluminum, $N(x)$, is represented by (Tasch et al., 1989)

$$N(x) = D_1 f_1(x) + D_2 f_2(x) \tag{17}$$

and

$$f_i(x) = K_i [1 + \{(x - R_{pi})/A_i - n_i/r_i\}^2]^{-mi} \exp[-n_i \arctan\{(x - R_{pi})/A_i - n_i/r_i\}^2] \quad (i = 1, 2), \tag{18}$$

where $f_1$ and $f_2$ are, respectively, normalized Pearson IV distribution functions for the randomly scattered and channeled components of the profile, and $D_1$ and $D_2$ are the doses represented by each Pearson function. For Pearson IV functions, $K_1$ and $K_2$ are normalized constants. $R_{p1}$ and $R_{p2}$ are projected ranges, and $n_1$, $n_2$, $r_1$, $r_2$, $A_1$, $A_2$, $m_1$, and $m_2$ are parameters related to the range stragglings $\Delta R_{p1}$ and $\Delta R_{p2}$, skewnesses $\gamma_1$ and $\gamma_2$, and kurtoses $\beta_1$ and $\beta_2$, as follows:

$$r_i = -(2 + 1/b_{2i}) \tag{19a}$$

$$n_i = -r_i\, b_{1i}/\sqrt{4\, b_{0i}\, b_{2i} - b_{1i}^2} \tag{19b}$$

$$m_i = -1/(2\, b_{2i}) \tag{19c}$$

$$A_i = m_i\, r_i\, b_{1i}/n_i \tag{19d}$$

$$b_{0i} = -\Delta R_{pi}^2\, (4\, \beta_i - 3\, \gamma_i^2)\, C \tag{19e}$$

$$b_{1i} = -\gamma_i\, \Delta R_{pi}\, (\beta_i + 3)\, C \tag{19f}$$

$$b_{2i} = -(2\, \beta_i - 3\, \gamma_i^2 - 6)\, C \tag{19g}$$

$$C = 1/[2\, (5\, \beta_i - 6\, \gamma_i^2 - 9)] \quad (i = 1, 2) \tag{19h}$$

Dose ratio, $R$, is defined as

$$R = D_1 \,/\, (D_1 + D_2). \tag{20}$$

To avoid arbitrariness of $R_{p2}$ (Suzuki et al., 1998), $R_{p2}$ was set equal to $R_{p1}$.

(d) Discussion

To understand the influence of the implantation energy sequence and the surface $SiO_2$ layer on channeling, BCA simulation of single-energy aluminum implantations into 4H-SiC were carried out, and the parameters of the dual Pearson model were fitted to the simulated data (Mochizuki et al., 2008). Concentration profiles of aluminum implanted with and without the $SiO_2$ layer are shown in Fig. 15. At an implantation energy of 35 keV, the profile of aluminum implanted with the $SiO_2$ layer becomes shallower than that without the $SiO_2$ layer when the aluminum concentration is more than $1\times10^{15}$ cm$^{-3}$. On the other hand, at an implantation energy of 70 keV or more, the profile of aluminum implanted without the $SiO_2$ layer becomes shallower than that with the $SiO_2$ layer when the aluminum concentration is less than $1\times10^{17}$ cm$^{-3}$. It is therefore concluded that in the case of the 35-nm-thick $SiO_2$ layer, the implantation energy at which the scatter-in channeling becomes more influential than the amorphization-suppressed channeling is between 35 and 70 keV.

The dual-Pearson parameters used to reproduce profiles in Fig. 15 are shown in Fig. 16, together with the reported parameters for single-Pearson models (Janson et al., 2003b; Stief et al. 1998; Lee and Park, 2002). Comparing the dual-Pearson parameters with the single-Pearson parameters shows that the dependences of $R_p$ in the case of implantation without the $SiO_2$ layer, $\Delta R_{p1}$, and $r_1$ are almost the same as those stated in two reports (Janson et al., 2003b; Stief et al., 1998) but slightly differ from those stated in another report (Lee and Park, 2002). Although the $\beta$'s of the reported single-Pearson model are not shown (to avoid complexity), the obtained relationship between $\beta_1$ and $r_1$ in Fig. 16(e),

$$\beta_1 = 1.19\, \beta_{1o} \tag{21a}$$

$$\beta_{1o} = [39\gamma_1^2 + 48 + 6(\gamma_1^2 + 4)^{3/2}] \,/\, (32 - \gamma_1^2), \tag{21b}$$

is very similar to the following reported relationship (Lee and Park, 2002):

$$\beta = 1.30\, \beta_o. \tag{21c}$$

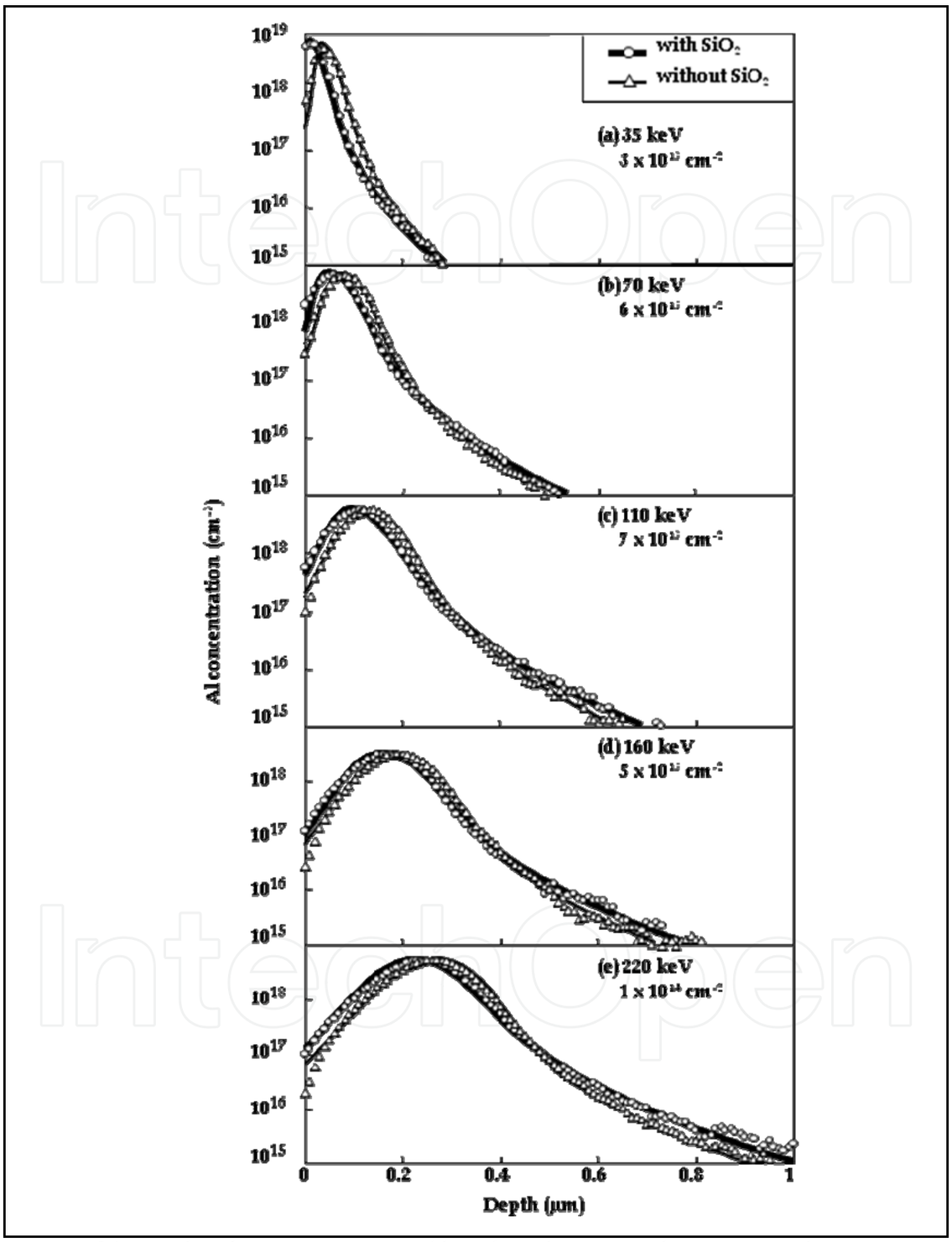


Fig. 15. BCA-simulated concentration profiles of single-energy aluminum implantations into 4H-SiC

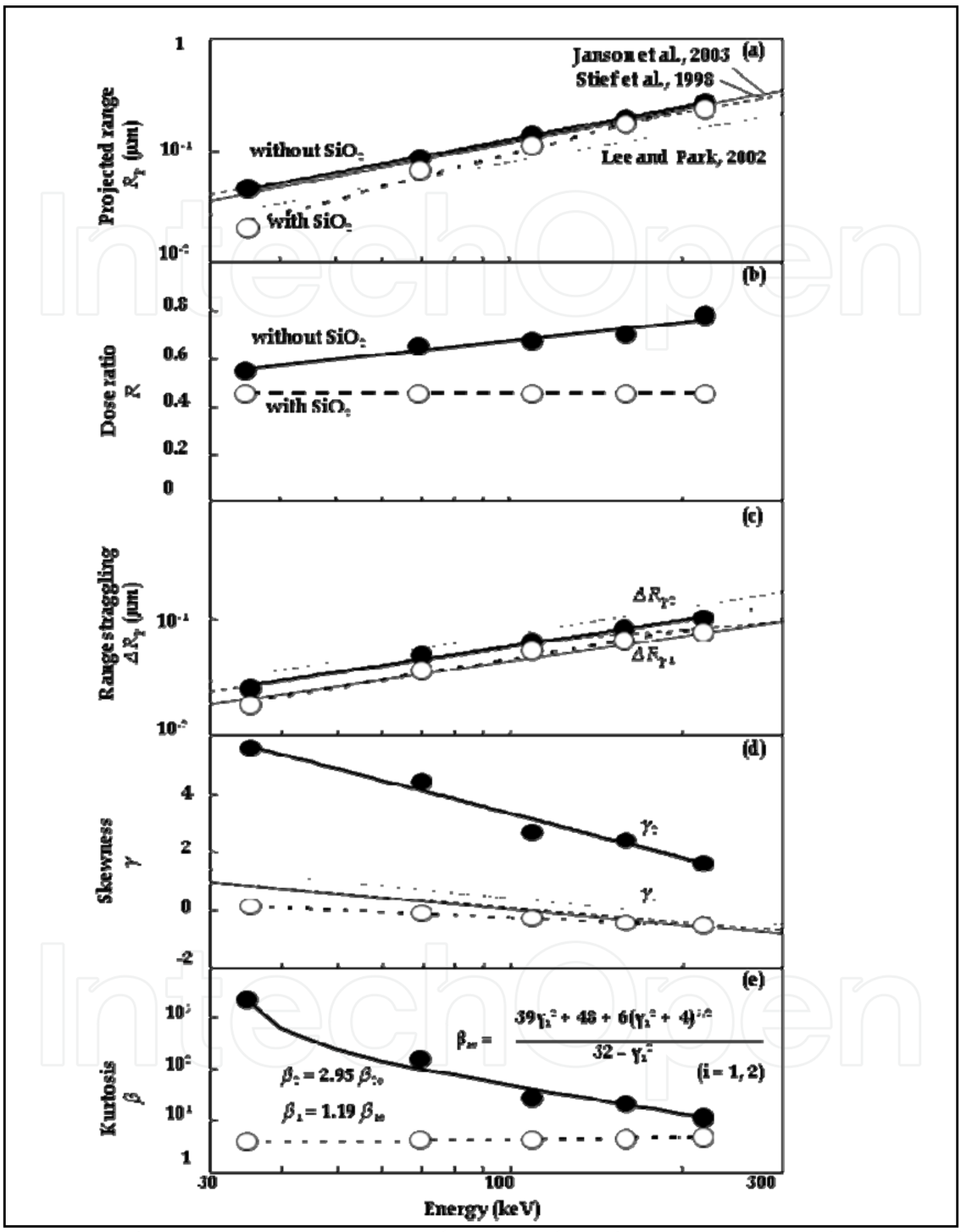


Fig. 16. Dual-Pearson parameters as a function of implantation energy (The projected ranges, range stragglings, and skewnesses from previous reports are also shown for comparison.)

In Fig. 16(a), $R_p$ for implantations with the $SiO_2$ layer is smaller than that for implantations without the $SiO_2$ layer. This result is due to the existence of the $SiO_2$ layer during implantation. On the other hand, in Fig. 16(b), compared to $R$ for implantations without the $SiO_2$ layer, $R$ for implantations with the $SiO_2$ layer becomes smaller, i.e., more aluminum ions channel, owing to the scatter-in channeling. It should be noted that in the case of aluminum implantations with the 35-nm-thick $SiO_2$ layer, $R$ monotonically increases under the following conditions (Mochizuki and Onose, 2007):

(1) dose of $1\times10^{14}$ $cm^{-2}$ and energy exceeding 300 keV, and
(2) dose of $1\times10^{15}$ $cm^{-2}$ or more and energy of 35 keV or more.

The influence of the amorphization-suppressed channeling (Ottaviani et al., 1999) might also increase under these conditions. To further investigate the effect of $SiO_2$, BCA simulation of 220-keV aluminum implantations through 0−40 nm $SiO_2$ layers was carried out, and the results were fitted with the dual-Pearson model using parameters shown in Figs. 16(c)–(e). With increasing thickness of the $SiO_2$ layer, $R_p$ monotonically decreases, while the decrease in $R$ tends to saturate (Fig. 17). The latter results may be helpful to understand the scatter-in channeling. Even in the case of implantation without the $SiO_2$ layer, $R$ is not unity; 20% of the impinging aluminum ions channel because the ions basically encounter random atoms in the outermost part of the 8°-off 4H-SiC itself. This scatter-in effect is enhanced with increasing $SiO_2$ layer thickness until it saturates around 35 nm. This indicates that the thickness of 35 nm is sufficient to maximize the $SiO_2$-layer-induced scatter-in channeling at an implantation energy of 220 keV.

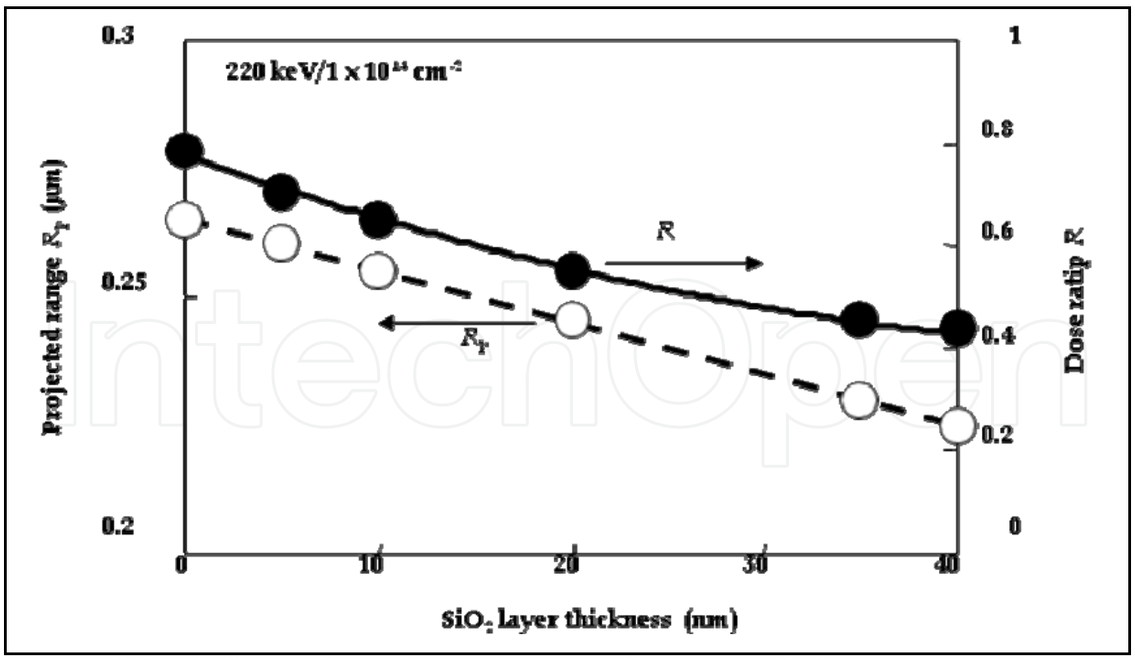


Fig. 17. $SiO_2$ thickness dependence of projected range and dose ratio for aluminum implantations at 220 keV with dose of 1 x $10^{14}$ $cm^{-2}$

On the basis of the above discussion of single-energy aluminum implantations into 4H-SiC, the tail in concentration profiles of multiple-energy aluminum implantations is discussed in the following. The symbols in Fig. 18 represent BCA-simulated profiles of aluminum implantations (a) without and (b) with the 35-nm-thick $SiO_2$ layer shown in Figs. 13 and 14. Concentration profiles of 220-keV implantations mainly determine the tail of the five-fold aluminum implantation, so the BCA-simulated results in Fig. 18 were fitted by varying $R$ for 220-keV implantations only. In the case of the aluminum implantations without $SiO_2$ layers [Fig. 18(a)], $R$ does not change from 0.78 in Fig. 16(b) for a decreasing energy order because the concentration profile in the first energy step (220 keV) determines the tail of the resultant five-fold implantation. On the other hand, $R$ decreases to 0.60 for an increasing energy order, meaning that the amount of channeling during the final energy step (220 keV) increases from that during the single-energy implantation at 220 keV. This result indicates that partially amorphized SiC causes the scatter-in channeling.

In the case of aluminum implantations with the 35-nm-thick $SiO_2$ layer [Fig. 18(b)], BCA simulation exhibits a tendency opposite to that observed in Fig. 18(a). The concentration profile of aluminum implantations performed in increasing order of energy results in a slightly less extended tail compared to that of aluminum implantations performed in decreasing order of energy. In the case of increasing order of implantation energy, $R$ increases to 0.57, and $R$ for the decreasing energy order does not change from 0.45 in Fig. 16(b). However, the former value is still lower than $R$ = 0.78 for the implantation without $SiO_2$ in a decreasing energy order [Fig. 18(b)]. This result indicates that although the amorphization-suppressed channeling (Ottaviani et al., 1999) occurred for implantations without $SiO_2$, the influence of the amorphization-induced scatter-in channeling is much larger.

When the two aluminum concentration profiles in Fig. 18(a) are compared vertically at a certain depth, the influence of channeling discussed above seems to be small. However, when they are compared horizontally, in the case of drift-layer doping in the order of $10^{15}$ $cm^{-3}$, the position of p-n junctions has about 10% error. The results in Fig. 18(a) also suggest that in the case of implantations without the $SiO_2$ layer in decreasing order of energy, concentration profiles of multiple-energy implantations can be obtained by simple summation of concentration profiles of single-energy implantations.

## 4. Conclusion and Future Studies

Diffusion and segregation of p-type dopants in 4H-SiC have been one-dimensionally modeled. Future studies should be directed toward two-dimensional models, which are challenging because of the great increase in the amount of data. The first two-dimensional model of aluminum-ion implantation into 4H-SiC (Mochizuki, K. & Yokoyama, N. 2011a and 2011b) is based on Monte-Carlo simulation, which revealed that iso-concentration contours of aluminum are independent of the orientation of the masking edge, as long as the aluminum dose is moderate ($10^{11}$ to $10^{13}$ $cm^{-2}$). Lateral range straggling can be extracted by expressing the lateral-concentration profiles as a one-dimensional dual-Pearson-distribution function multiplied by a Gaussain distribution function. Such a two-dimensional model should contribute to efficiently simulating the current-voltage characteristics of 4H-SiC power devices.

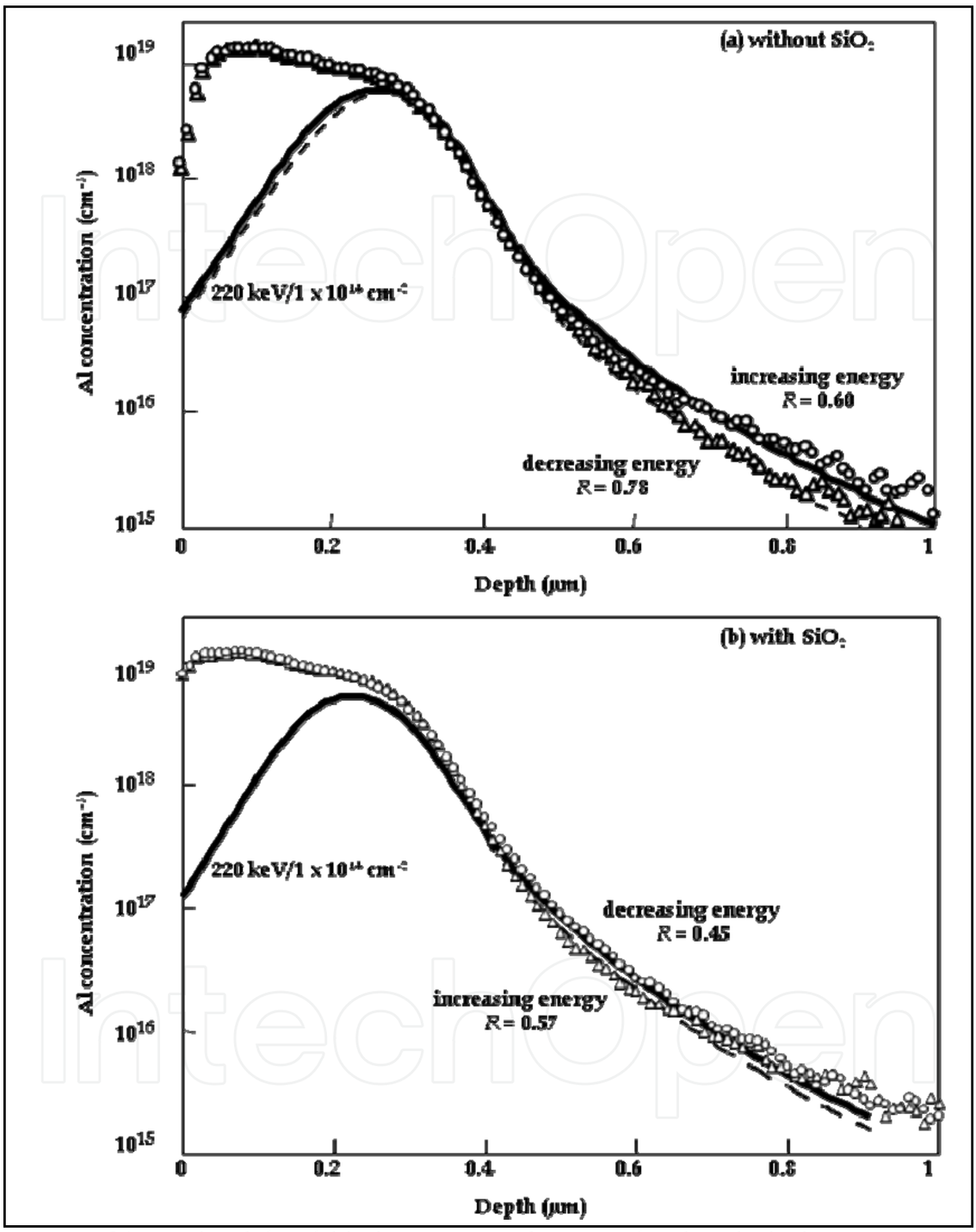


Fig. 18. BCA-simulated five-fold aluminum implantation fitted with dual-Pearson model with dose ratio of 220-keV implantation as parameter

## 5. References

Aradi, B., Gali, A., Deák, P., Rauls, E., Frauenheim, Th. & Son, N.T. (2001). Boron centers in 4H-SiC. *Materials Science Forum,* Vol. 353-356, (2001) 455-458, 0255-5476

Baliga, B. J. (2005). *Silicon Carbide Power Devices,* World Scientific, 978-981-256-605-8, Singapore

Bockstedte, M., Mattausch, A. & Pankratov, O. (2001). Boron in SiC: structure and kinetics. *Materials Science Forum,* Vol. 353-356, (2001) 447-450, 0255-5476

Bockstedte, M., Mattausch, A. & Pankratov, O. (2003). Ab initio study of the migration of intrinsic defects in 3C-SiC. *Physical Review B,* Vol. 68, No. 20 (Nov. 2003) 205201, 1098-0121

Bockstedte, M., Mattausch, A. & Pankratov, O. (2004). Different roles of carbon and silicon interstitials in the interstitial-mediated boron diffusion in SiC. *Physical Review B,* Vol. 70, No. 11 (Sept. 2004) 205201, 1098-0121

Bracht, H., Stolwijl, N. A. & Pensl, G. (2000). Diffusion of boron in silicon carbide: evidence for the kick-out mechanism. *Applied Physics Letters,* Vol. 77, No. 20, (Nov. 2000) 3188-3120, 0003-6951

Bracht, H. (2007). Self- and foreign-atom diffusion in semiconductor isotope heterostructures. I. Continuum theoretical calculations. *Physical Review B,* Vol. 75, No. 3 (Jan. 2007) 035210, 1098-0121

Chakarov, I. & Temkin, M. (1999). Modelling of ion implantation in SiC crystals, *Nuclear Instruments and Methods in Physics Research, Section B: Beam Interactions with Materials and Atoms,* Vol. 242, No. 1-2, (2006) 690-692, 0168-583X

Cho, Y., Zographos, N., Thirupapulivur, S. & Moroz, V. (2007). Experimental and theoretical analysis of dopant diffusion and C evolution in hjigh-C Si :C epi layers: optimazation of Si :C source and drain formed by post-epi implant and activation anneal, *Technical Digest of International Electron Devices Meeting*, pp. 959-962, 978-1-4244-1507-6, Washington, D.C., Dec. 2007, IEEE, Piscataway

Duijin-Arnold, A. v., Ikoma, T., Poluektov, O. G., Baranov, P. G., Mokhov, E. N. & Schmidt, J. (1998). Electronic structure of the deep boron acceptor in boron-doped 6H-SiC. *Physical Review B,* Vol. 57, No. 3 (Jan. 1998) 1607-1619, 1098-0121

Duijin-Arnold, A. v., Mol., J., Verberk, R., Schmidt, J., Mokhov, E.N. & Baranov, P. G. (1999). Spatial distribution of the electronic wave function of the shallow boron acceptor in 4H- and 6H-SiC. *Physical Review B,* Vol. 60, No. 23 (Dec. 1999) 15829-15847, 1098-0121

Gao, F., Weber, W. J., Posselt, M. & Belko, V. (2004). Atomistic study of intrinsic defect migration in 3C-SiC. *Physical Review B,* Vol. 69, No. 24 (June 2004) 245205, 1098-0121

Heera, V., Panknin, D. & Skorupa, W. (2001). P-type doping of SiC by high dose Al implantation−Problems and progress. *Applied Surface Science,* Vol. 184, No. 1−4, (Dec. 2001) 307−316, 0169-4332

Hoshi, M., Hayashi, Y., Tanaka, H. & Yamagami, S. (2007). Novel SiC power devices utilizing a Si/4H-SiC heterojunction, *Proceedings of Power Conversion Conference*, pp. 373-376, 1-4244-0844-X, Nagoya, April 2007, IEEE, Piscataway

Janson, M.S., Linnarsson, M.K., Hallén, A. & Svensson, B.G. (2003a). Transient enhanced diffusion of implanted boron in 4H-silicon carbide. *Applied Physics Letters,* Vol. 76, No. 11, (March 2003) 1434-1436, 0003-6951

Janson, M.S., Linnarsson, M.K., Hallén, A. & Svensson, B.G. (2003b). Ion implantation range distributions in silicon carbide. *Journal of Applied Physics,* Vol. 93, No. 11, (June 2003) 8903-8909, 0021-8979

Kinchin, G.H. & Pease, R.S. (1955). The displacement of atoms in solids by radiation. *Reports on Progress in Physics,* Vol. 18, (1955) 1-51, 0034-4885

Kuroda, N., Shibahara, K., Yoo, W.S., Nishino, S. & Matsunami, H. (1987). Step-controlled VPE growth of SiC single crystals at low temperatures, *Extended Abstracts of 19th Conference on Solid State Devices and Materials*, pp. 227-230, Tokyo, 1987, Japan Society of Applied Physics, Tokyo

Lau, F. (1990). Modeling of polysilicon diffusion sources, *Technical Digest of International Electron Devices Meeting*, pp. 67-70, 0163-1918, San Francisco, Dec. 1990, IEEE, Piscataway

Lee, S.-S. & Park, S.-G. (2002). Empirical depth profile model for ion implantation in 4H-SiC. *Journal of Korean Physical Society,* Vol. 41, No. 5, (Nov. 2002) L591-L593, 0374-4884

Linnarsson, M. K., Janson, M. S., Shoner, A. & Svensson, B.G. (2003). Aluminum and boron diffusion in 4H-SiC, *Materials Research Society Proceedings*, Vol. 742, paper K6.1, 1-55899-679-6, Warrendale, Dec. 2002, Materials Research Society, Boston

Linnarsson, M.K., Janson, M.S., Schnöer, A., Konstantinov, A. & Svensson, B.G. (2004). Boron diffusion in intrinsic, n-type amd p-type 4H-SiC. *Materials Science Forum,* Vol. 457-460, (2004) 917-920, 0255-5476

Linnarsson, M.K., Janson, M.S., Nordell, N., Wong-Leung, J. & Schöner, A. (2006). Formation of precipitates in heavily boron doped 4H-SiC. *Applied Surface Science,* Vol. 252, ( 2006) 5316-5320, 0169-4332

Liu, C.-I., Windl, W., Borucki, L. & Lu, S. (2002). Ab initio modeling and experimental study of C-B interactions in Si. *Applied Physics Letters,* Vol. 80, No. 1, (Jan. 2002) 52-54, 0003-6951

Mochizuki, K. & Onose, H. (2007). Dual-Pearson approach to model ion-implanted Al concentration profiles for high-precision design of high-voltage 4H-SiC power devices, *Technical Digest of International Conference on Silicon Carbide and Related Materials*, pp. Fr15-Fr16 (late news), Otsu, Oct. 2007

Mochizuki, K., Someya, T., Takahama, T., Onose, H. & Yokoyama, N. (2008). Detailed analysis and precise modelling of multiple-energy Al implantations through $SiO_2$ layers into 4H-SiC. *IEEE Transactions on Electron Devices,* Vol. 55, No. 8, (Aug. 2008) 1997-2003, 0018-9383

Mochizuki, K., Shimizu, H. & Yokoyama, N. (2009). Dual-sublattice modeling and semi-atomistic simulation of boron diffusion in 4H-slicon carbide. *Japanese Journal of Applied Physics,* Vol. 48, No. 3, (March 2009) 031205, 021-4922

Mochizuki, K., Shimizu, H. & Yokoyama, N. (2010). Modeling of boron diffusion and segregation in poly-Si/4H-SiC structures. *Materials Science Forum,* Vol. 645-648, (2010) 243-246, 0255-5476

Mochizuki, K. & Yokoyama, N. (2011a). Two-dimensional modelling of aluminum-ion implantation into 4H-SiC. To be published in *Materials Science Forum*; presented at *European Conference on Silicon Carbide and Related Materials*, paper WeP-47, Oslo, Aug. 2010

Mochizuki, K. & Yokoyama, N. (2011b). Two-dimensional analytical model for concentration profiles of aluminium implanted into 4H-SiC (0001). To be published in *IEEE Transactions on Electron Devices*, Vol. 58, (2011), 0018-9383

Mokhov, E.N., Goncharov, E.E. & Ryabova, G.G. (1984). Diffusion of boron in p-type silicon carbide. *Soviet Physics - Semiconductors,* Vol. 18, (1984) 27-30, 0038-5700

Morris, S.J., Yang, S.-H., Lim, D.H., Park, C., Klein, K.M., Manassian, M. & Tasch, A.F. (1995). An accurate and efficient model for boron implants through thin oxide layers into single-crystal silicon. *IEEE Transactions on Semiconductor Manufacturing,* Vol. 8, No. 4, (Nov. 1995) 408-413, 0894-6507

Ottaviani, L., Morvan, E., Locatelli, M.-L.., Planson, D., Godignon, P., Chante, J.-P. & Senes, A. (1999). Aluminum multiple implantations in 6H-SiC at 300K. *Solid-State Electronics,* Vol. 43, No. 12, (Dec. 1999) 2215-2223, 0038-1101

Park, C., Klein, K., Tasch, A., Simonton, R. & Lux, G. (1991). Paradoxical boron profile broadening caused by implantation through a screen oxide layer, *Technical Digest of International Electron Devices Meeting*, pp. 67-70, 0-7803-0243-5, Washington, D.C., Dec. 1991, IEEE, Piscataway

Pearson, K. (1895). Contributions to the mathematical theory of evolution, II: skew variation in homogeneous material. *Philosophical Transactions of the Royal Society of London, A,* Vol. 186, (1895) 343-414, 0080-4614

Plummer, G. H., Deal, M. D. & Griffin, P. B. (2000). *Silicon VLSI Technology*, 411, Prentice Hall, 9780130850379, Upper Saddle River

Rausch, W.A., Lever, R.F. & Kastl, R.H. (1983). Diffusion of boron into polycrystalline silicon from a single crystal source. *Journal of Applied Physics,* Vol. 54, No. 8, (Aug. 1983) 4405-4407, 0021-8979

Rurali, R., Godignon, P., Rebello, J., Ordejón, P. & Hernández, E. (2002). Theoretical evidence for the kick-out mechanism for B diffusion in SiC. *Applied Physics Letters,* Vol. 81, No. 16, (Oct. 2002) 2989-2991, 0003-6951

Rüschenschmidt, K., Bracht, H., Stolwijk, N. A., Laube, M., Pensl, G. & Brandes, G. R. (2004). Self-diffusion in isotopically enriched silicon carbide and its correlation with dopant diffusion. *Journal of Applied Physics,* Vol. 96, No. 3, (Aug. 2004) 1458-1463, 0021-8979

Sadigh, B., Lenosky, T. J., Theiss, S. K., Caturla, M.-J., de la Rubia, T. D. & Foad, M. A. (1999). Mechanism of boron diffusion in silicon: an ab initio and kinetic Monte Carlo study. *Physical Review Letters,* Vol. 83, No. 21 (Nov. 1999) 4341-4344, 0031-9007

Srindhara, S. G., Clemen, L. L., Devaty, R. P., Choyke, W. J., Larkin, D. J., Kong, H. S., Troffer, T. & Pensl, G. (1998). Photoluminescence and transport studies of boron in 4H-SiC. *Journal of Applied Physics,* Vol. 83, No. 12, (Jan. 1998) 7909-7920, 0021-8979

Stewart, E.J., Carroll, M.S. & Sturm, J.C. (2005). Boron segregation in single-crystal $Si_{1-x-y}Ge_xC_y$ and $Si_{1-y}C_y$ alloys. *Journal of Electrochemical Society,* Vol. 152, (2005) G500, 0013-4651

Stief, R., Lucassen, M., Schork, R., Ryssel, H., Holzlein, K.-H., Rupp, R. & Stephani, D. (1998). Range studies of aluminum, boron, and nitrogen implants in 4H-SiC, *Proceedings of International Conference on Ion Implantation Technology*, pp. 760-763, 0-7803-4538-X, Kyoto, June 1998, IEEE, Piscataway

Suzuki, K., Sudo, R., Tada, Y., Tomotani, M., Feudel, T. & Fichtner, W. (1998). Comprehensive analytical expression for dose dependent ion-implanted impurity concentration profiles. *Solid-State Electronics,* Vol. 42, No. 9, (Sept., 1998) 1671-1678, 0038-1101

Tasch, A.F., Shin, H., Park, C., Alvis, J. & Novak, S. (1989). An improved approach to accurately model shallow B and $BF_2$ implants in silicon. *Journal of Electrochemical Society,* Vol. 136, No. 3, (1989) 810-814, 0013-4651

Tsirimpis, T., Krieger, M., Weber, H.B. & Pensl, G. (2010). Electrical activation of $B^+$-ions implanted into 4H-SiC. *Materials Science Forum,* Vol. 645-648, (2010) 697-700, 0255-5476

Windle, W., Bunea, M.M., Stumpf, R., Dunham, S.T. & Masquelier, M.P. (1999). First-principles study of boron diffusion in silicon. *Physical Review Letters,* Vol. 83, No. 21 (Nov. 1999) 4345-4348, 0031-900

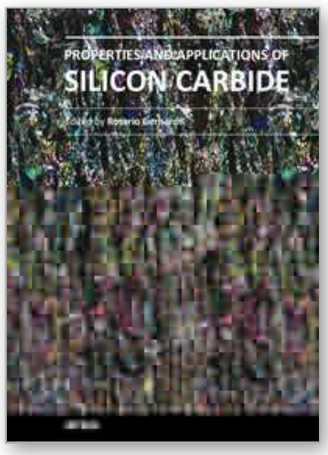


**Properties and Applications of Silicon Carbide**

Edited by Prof. Rosario Gerhardt

ISBN 978-953-307-201-2
Hard cover, 536 pages
**Publisher** InTech
**Published online** 04, April, 2011
**Published in print edition** April, 2011

In this book, we explore an eclectic mix of articles that highlight some new potential applications of SiC and different ways to achieve specific properties. Some articles describe well-established processing methods, while others highlight phase equilibria or machining methods. A resurgence of interest in the structural arena is evident, while new ways to utilize the interesting electromagnetic properties of SiC continue to increase.



**InTech Europe**
University Campus STeP Ri
Slavka Krautzeka 83/A
51000 Rijeka, Croatia
Phone: +385 (51) 770 447
Fax: +385 (51) 686 166
www.intechopen.com

**InTech China**
Unit 405, Office Block, Hotel Equatorial Shanghai
No.65, Yan An Road (West), Shanghai, 200040, China
中国上海市延安西路65号上海国际贵都大饭店办公楼405单元
Phone: +86-21-62489820
Fax: +86-21-62489821

IntechOpen